



# PV BASED DC-DC CONVERTER FOR INDUCTION MOTOR DRIVE APPLICATION

P.PRAGNA

M-tech Student Scholar

Department of Electrical & Electronics Engineering,  
Narasaraopet Engineering College, Narasaraopet;  
Guntur (Dt); A.P, India.

Dr.P.Lakshmanan M.E,Ph.D

Professor

Department of Electrical & Electronics Engineering,  
Narasaraopet Engineering College, Narasaraopet;  
Guntur (Dt); A.P, India

**Abstract**-Renewable energy sources (RES's) is the major source of electrical energy in future, the available renewable energy systems are solar, wind, fuel cell out of these solar system is most popularly used because this source hugely available in nature, this renewable energy source (RES) is most in demand for agricultural, industrial applications. In the agricultural field renewable energy source (RES) is feeding the motor, to have high efficiency for the motor. Motor is design for high voltage, where as to have high efficiency for solar system it is designed for low voltage. SO we need low voltage to high voltage converter. Various high voltage gain dc-dc converters are proposed in the literature out of those hybrid boost converter is chosen because of its simplicity and high voltage gain. This paper mainly proposes the integration of PV system with dc-dc converter and dc-ac inverter feeding an induction motor drive. Maximum power point tracking algorithm (Perturb & Observe) is used to extract maximum power from photovoltaic panel. When the interface converter operates in OVR mode, PV cells can only operate stably in voltage area or current area. Moreover, the type of operating area entirely depends on the converter's output voltage control loop formation. The converter is controlled on closed loop to maintain output voltage constant. Even inputs sun radiations are varying. A Mat lab/Simulink models are developed for high gain dc-dc converter drive applications.

**Key words:** DC-DC converters, Induction motor, RES's, Maximum Power Point Tracking (MPPT).

## I. INTRODUCTION

PV power systems are efficient alternate source to provide electrical energy. But the drawback with the PV system is high installation cost to decreases the installation cost we need to increase the efficiency of the PV system required the P.E interface. Most commonly boost converter is used but as gain of dc-dc [1-2] converter increase its efficiency also increase. There are several converters are proposed in the literature to increase the voltage gain. Mainly dc- dc converters are classified into 2 types

1. Non – isolated dc-dc converters
2. Isolated dc-dc converters

The advantage of non-isolated dc- dc converters simple and low cost but disadvantage is its voltage gain is limited. The advantage of isolated dc-dc converter is high voltage gain but it has a disadvantage of high cost and more components. In the literature a hybrid boost converter is proposed to increase the voltage gain with simple structure [3-5]. In many industries induction motor drive is used because of its low cost and low maintenance. Induction motors are design for high voltage to have high efficiency.

By integrating the PV system we can reduce the energy consumption for integrating this PV system we are using a high voltage gain hybrid dc-dc converter and 3-level diode clamped inverter [6]. This work mainly focusing on integration of PV system with the induction motor using closed loop controlled hybrid dc-dc converter [7-8]. This paper explains the effective operation of Induction motor is based on the choice of suitable high voltage gain converter system that is fed to Induction Motor. Here the induction motor drive is control action is done with closed loop mode of system.

Photovoltaic power provides an environment friendly green source of electricity, of which the fuel is sunrays, a renewable energy [9]. However, widespread use of fossil fuels has caused environmental pollution especially emission of Carbon-di-oxide from vehicles and power plants, that affect the global climate and temperature. The human concern for the environment and the way our modern technology deteriorates has aroused scientists and engineers all over the world to explore the cleaner renewable energy based electricity generation. Photovoltaic (PV) is one such technology first observed and Implemented by Alexander-Edmond Becquerel in 1839, where solar energy is converted to electricity.

A power electronics interface is essential in order to run the three-phase induction motor using the solar panel. Thus using power electronics interface like dc-dc push-pull converter merge with a multilevel inverter, it is possible to transfer the power efficiently from the panel to the machine useable sinusoidal ac with the help of



Maximum Power Point Tracking (MPPT) [10], where MPPT works by changing the parameters of the power electronics components in order to obtain the maximum power available at that moment of the panel. Hence, Perturb and Observe (P&O) technique is implemented to accomplish this task. According to researchers [11], Pulse Width Modulation (PWM) technique is used for inverter switching and controlling of induction motor. It implies that the control loop formation may be the real reason leading to the difference of stable operating area between these two schemes.

Hence, this paper investigates in depth in the relations between control loop formation of the interface converter in OVR [12] mode and the stable operating area of PV cells and on this basis replies unambiguously to the above questions.

**II. CONTROL STRATEGY OF PV INTERFACE CONVERTER**

Fig.1 shows the basic configuration of PV power generation system, where both the input voltage  $u_{in}$  and the output voltage  $u_o$  of the interface converter are sampled and controlled. The input voltage controller and the output voltage controller should be arranged to work separately (see Fig. 2a), in cascade (see Fig. 2b) or in series (see Fig. 2c) [8, 12]. In Fig. 2, both symbol ‘\*’ and symbol ‘\*\*’ represent the operation symbol (+ or -), while the operations of ‘\*’ and ‘\*\*’ are always inverse. The output voltage reference  $u_{o,ref}$  predefined in Fig. 2 represents the over voltage protect threshold  $U_{o,max}$  of the interface converter. The function Select {1, 2} shown in Figs. 2a and c is used to select the larger (or the smaller) one between branch 1 and branch 2. In Fig. 2b, the Limit {1} is a function to limit the maximum (or the minimum) output to be zero. The functions of Limit {1} and Select {1, 2} depend on the output voltage feedback control method. Table 1 shows the relations between the output voltage feedback control method and the functions of Limit {1} and Select {1, 2}.

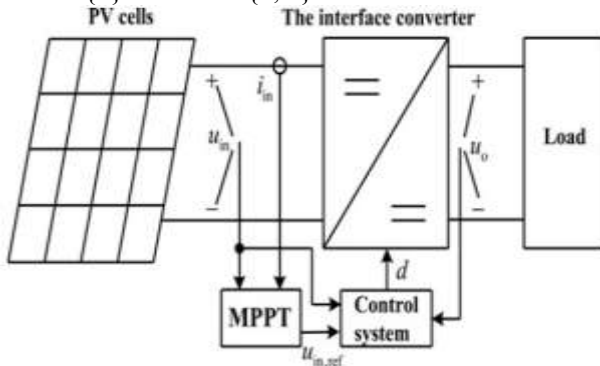
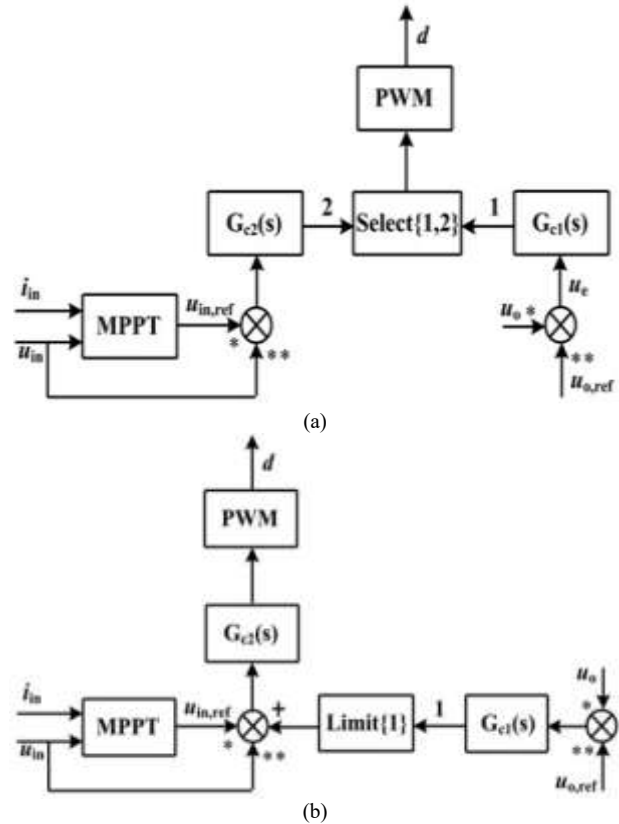


Fig.1 PV power generation system's structure

With the help of such functions, the interface converter can automatically switch operating modes between MPPT and OVR. For example, as shown in Fig. 2a and Table 1, if the feedback control method is  $u_e = u_o, ref - u_o$ , Select {1, 2} should be a function to select the smaller output value between branch 1 and 2. Then, when  $u_o$  is lower than  $U_{o,max}$ , the output voltage controller  $G_{c1}(s)$  [generally as a proportional-integral (PI) controller] will output the positive saturation value which is larger than the output of controller  $G_{c2}(s)$ . Obviously, the branch 2 (the input voltage controller) is chosen and the converter works in MPPT mode in such case. Once  $u_o$  reaches  $U_{o,max}$ ,  $G_{c1}(s)$  begins



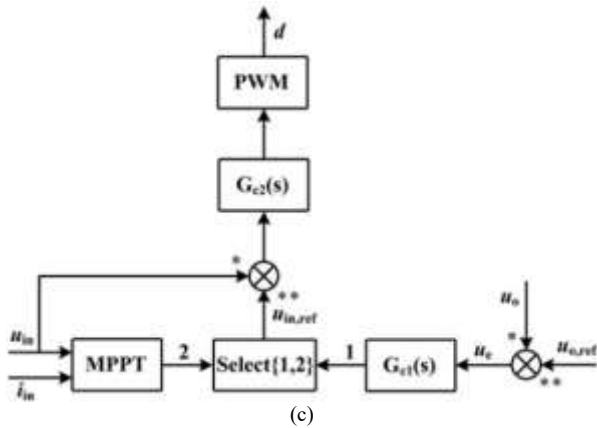


Fig. 2 Control system arrangements (a) Separate controllers (b) Cascaded controllers (c) Series controllers

Table 1 Relations between the output voltage feedback control method and the functions of Limit {1} and Select {1, 2} to exit saturation and then its output will persistently decrease from the saturation value. Finally, it will fall below the output of Gc2(s) and branch 1 will be selected. As a result, the converter begins to work in OVR mode.

Table 1: Relations between the output voltage feedback control method

Control system arrangements	Feedback control methods	Functions
separate controllers	$u_e = u_{o,ref} - u_o$	Select (1, 2) select the smaller one between branch 1 and branch 2
	$u_e = u_o - u_{o,ref}$	Select (1, 2) select the larger one between branch 1 and branch 2
cascaded controllers	$u_e = u_{o,ref} - u_o$	Limit {1} limit the maximum output to be zero
	$u_e = u_o - u_{o,ref}$	Limit {1} limit the minimum output to be zero
series controllers	$u_e = u_{o,ref} - u_o$	Select (1, 2) select the smaller one between branch 1 and branch 2
	$u_e = u_o - u_{o,ref}$	Select (1, 2) select the larger one between branch 1 and branch 2

III. SMALL-SIGNAL MODELLING OF BOOST CONVERTER WITH AN INPUT CAPACITOR

As the most common interface converter used in PV power generation systems, the boost converter with an input capacitor shown in Fig. 3 is taken as an example and analyzed in this work. Fig. 3a shows the PV system's

main circuit, where the dashed box indicates the equivalent circuit of the PV cells. Rd and Cd are the dynamic resistance and dynamic junction capacitance of the diodes in PV cells, respectively. Rd decreases with increasing the photocurrent Isc and the terminal voltage Uin, while Cd changes oppositely. The shunt resistance Rsh and series resistance Rs are to represent the various non-idealities of the real PV cells. Moreover, as seen from Fig. 3a, Cin is the input filter capacitor, Co is the output filter capacitor and L is the input filter inductor. To simplify the analysis, the parasitic parameters of all components are negligible.

In general, the load of PV interface converter can be divided into four common types: constant current load (Is), constant resistive load (R), quasi-constant voltage load (the series branch composed of voltage source Ub and its internal resistance Rb) and constant power load (P). Nevertheless, PV interface converter with constant power load can only work in OVR mode, not in MPPT mode. Since the converter needs to work in two modes, only the first three loads are analyzed in this paper. To avoid building repeatedly dynamic models of the system with different loads, all the three loads are taken together, as shown in Fig. 3a.

Small-signal analysis, featuring with easier modeling and access to the classical linear control theory, is the most common dynamic analytical method of power converter. It is very accurate when the disturbance is very small and its frequency is lower than 1/5fs – 1/2fs (fs is switching frequency). Hence, it is taken in this paper to investigate the stable operating area of PV cells feeding the interface converter in OVR mode.

In one switching cycle, suppose the boost converter operates around the steady-state operating point  $I_{sc}, U_{in}, I_{in}, I_L, U_o$  and  $D$ , with small-signal perturbation  $\hat{i}_{sc}, \hat{u}_{in}, \hat{i}_{in}, \hat{i}_L, \hat{u}_o$  and  $\hat{d}$  and  $d$ . Then, the equivalent circuit of the boost converter can be developed by the averaged switch modeling, as shown in Figs. 3b and c. The small-signal dynamic resistance Rd can be deduced by linearization of the diode in PV cells, as shown in Fig. 3d.

According to Fig. 3b, the steady-state operating point can be obtained as

$$\begin{cases} U_{in}(s) + D\bar{U}_0(s) + U_o\bar{d}(s) = sL\hat{i}_L(s) + \bar{U}_0(s) \\ \hat{i}_{sc}(s)Z_1(s) = \bar{U}_{in}(s)[1 + sC_{in}Z_0(s)] + \hat{i}_L(s)Z_0(s) \\ (1-D)\hat{i}_L(s)z_2(s) = I_{in}\bar{d}(s)z_2(s) + \bar{U}_0(s) \end{cases}$$



$$\begin{cases} U_{in} = U_0(1-D) \\ I_{SC} = \frac{R_d + R_{sh}}{R_d R_{sh}} (u_{in} + I_{in} R_0) \\ I_{in} = I_L \\ (1-D)I_L = I_0 \end{cases} \quad (1)$$

Where

$$R_0 = R_d / R_{sh} + R_s = \frac{R_d R_{sh} + R_s R_{sh} + R_s R_d}{R_{sh} + R_d}$$

From Fig.3c, the small-signal equations can be described as follows:

And  $\tau_n = R_d C_d$  is the minority carrier lifetime of the PV cells [the detailed derivation about  $Z_0(s)$  and  $\tau_n$  is given in [7, 20]].

Then, we can get

$$\begin{aligned} G_{UD1}(s) &= \left. \frac{U_0(s)}{d(s)} \right|_{i_{sc}(s)=0} = \frac{U_{in} Z_2(s) - I_{in} Z_2(s) [Z_3(s) + sL]}{(1-D)^2 Z_2(s) + Z_3(s) + sL} \\ G_{ud2}(s) &= \left. \frac{U_{in}(s)}{d(s)} \right|_{i_{sc}(s)=0} = - \frac{U_0 Z_3(s) + (1-D) I_{in} Z_2(s) Z_3(s)}{(1-D)^2 Z_2(s) + Z_3(s) + sL} \end{aligned} \quad (4)$$

Where

$$Z_3(s) = (Z_0(s) / (1 + sC_{in} Z_0(s)))$$

$$K_1 = \frac{R_{sh}}{R_{sh} + R_d},$$

$$Z_1(s) = R_d // R_{sh} // \frac{1}{sC_d} = \frac{R_{sh} R_d}{sT_n R_{sh} + R_{sh} + R_d},$$

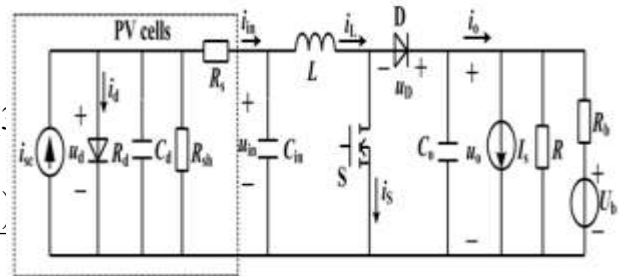
$$Z_2(s) = R // R_b // \frac{1}{sC_0} = \frac{RR_b}{sRR_b C_0 + R + R_b},$$

$$Z_0(s) = Z_1(s) + R_s = \frac{sT_n R_s K_1 + R_0}{sT_n K_1 + 1}$$

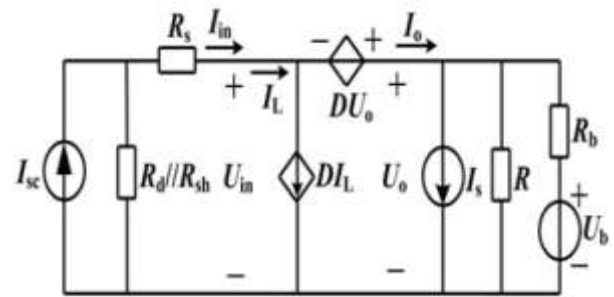
#### IV. OUTPUT VOLTAGE CONTROL STABILITY OF PV INTERFACE CONVERTER

##### a) Output voltage closed-loop control structure of the interface converter

As can be seen from Fig. 2, the output voltage closed-loop control system of PV interface converter can be classified into two basic structures: the output voltage single loop control (Fig. 2a) and the output–input voltage double loop control (Figs. 2b and c). Fig. 4 shows the block diagram of these two control structures, where  $K_{u1}$  and  $K_{u2}$  are, dth modulation (PWM) modulator gain, and  $G_{c1}(s)$  and  $G_{c2}(s)$  are, respectively, the transfer functions of the output voltage controller and the input voltage controller.



(a)



(b)

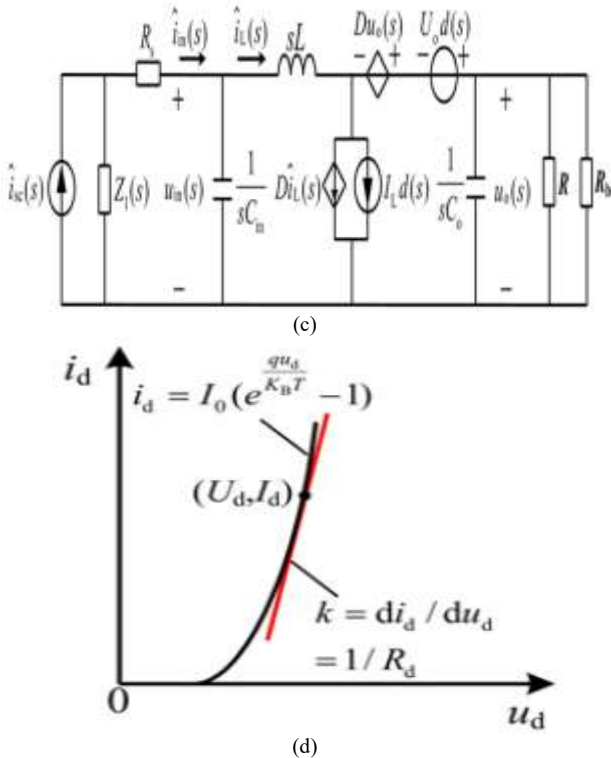


Fig. 3 Boost converter with PV cells' dynamic equivalent circuit model

(a) Main circuit (b) DC equivalent circuit (c) AC small-signal equivalent circuit (d) Linearization of the diode in PV cell

**b) Necessary stability condition for the output voltage single closed-loop control system**

From Fig. 4a, if '\*' represents '+' and '\*\*' represents '-', which means the feedback control method is  $\hat{e}_1(s) = \hat{u}_{0,ref}(s) - K_{u1}\hat{u}_0(s)$  then the closed-loop transfer function of the output voltage single loop control system can be obtained as

$$\frac{\hat{u}_0(s)}{\hat{u}_{0,ref}(s)} = \frac{F_m G_{c1}(s) G_{ud1}(s)}{1 + K_{u1} F_m G_{c1}(s) G_{ud1}(s)} \quad (5)$$

If PI regulation is adopted in this control system, we will have

$$G_{c1}(s) = K_{p1} + \frac{K_{i1}}{s} \quad (6)$$

Substituting (3) and (6) in (5), the characteristic equation of the single closed-loop system can be written as

$$a_0 s^5 + a_1 s^4 + a_2 s^3 + a_3 s^2 + a_4 s + a_5 = 0 \quad (7)$$

Where (see equation at the bottom of the next page)

Hurwitz stability criterion indicates that the necessary stability condition of linear system is that each coefficient of the characteristic equation is positive when  $a_0 > 0$ . Thus, to ensure the stability of the single loop control system, the following inequality has to be satisfied:

$$a_5 = K_{u1} F_m K_{i1} (U_{in} - I_{in} R_0) R R_b / (R + R_b) > 0 \quad (8)$$

Where both R and R<sub>b</sub> depend on the load type. For example, if the actual load type is constant current load, R and R<sub>b</sub> will be infinity.

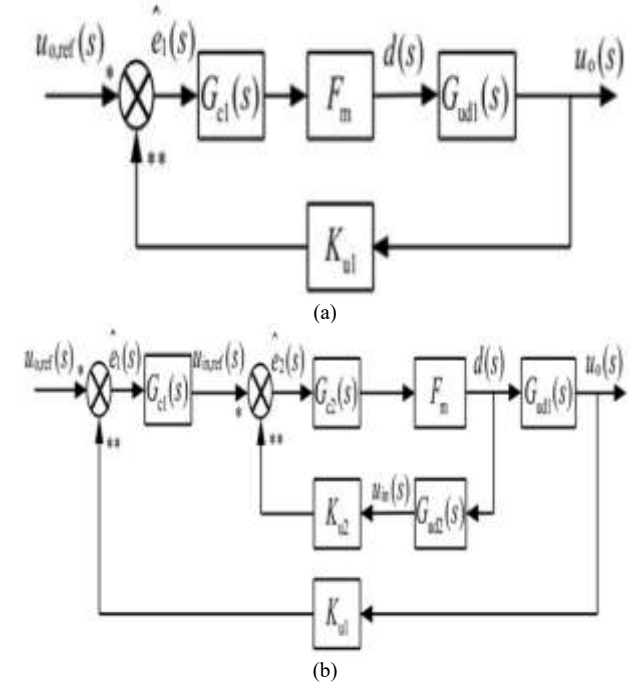


Fig. 4 Block diagram of output voltage closed-loop control (a) Single closed-loop control structure (b) Double closed-loop control structure

If the actual load type is constant resistance, then R is constant and R<sub>b</sub> will be infinity. While if the actual load type is quasi-constant voltage load, R will be infinity and R<sub>b</sub> keeps constant. However, whatever the load type is, we can have  $R R_b / (R + R_b) > 0$ . Hence

$$F_m (R_{in} - R_0) > 0 \quad (9)$$

Where  $R_{in} = U_{in}/I_{in}$  is the equivalent input resistance of PV interface converter. Obviously, inequality (9) is not related to the load type.

Similarly, if feedback control method is  $\hat{e}_1(s) = K_{u1}\hat{u}_0(s) - \hat{u}_{0,ref}(s)$ , there is

$$F_m (R_{in} - R_0) < 0 \quad (10)$$

**c) Necessary stability condition for the output- input voltage double closed-loop control system**



From Fig. 4b, if ‘\*’ in both control loops represent ‘+’ while ‘\*\*’ represent ‘-’, which means the feedback control method is

$$\begin{cases} \dot{e}_1(s) = \dot{u}_{0,ref}(s) - k_{u1}\dot{u}_0(s) \\ \dot{e}_2(s) = \dot{u}_{in,ref}(s) - k_{u2}\dot{u}_{in}(s) \end{cases}$$

Then the closed-loop transfer function of the output–input voltage double closed-loop control system can be obtained as

$$\frac{\dot{U}_0(s)}{\dot{U}_{0,ref}(s)} = \frac{F_m G_{c1}(s)G_{c2}(s)G_{ud1}(s)}{1 + F_m K_{u2} G_{c2}(s)G_{ud2}(s) + F_m K_{u1} G_{c1}(s)G_{c2}(s)G_{ud1}(s)} \quad (11)$$

If PI regulation is adopted in this control system, we will have

$$G_{c1}(s) = K_{p1} + \frac{K_{i1}}{s}, G_{c2}(s) = K_{p2} + \frac{K_{i2}}{s} \quad (12)$$

Substituting (3), (4) and (12) in (11), the characteristic equation of the system can be written as

$$a_0s^6 + a_1s^5 + a_2s^4 + a_3s^3 + a_4s^2 + a_5s + a_6 = 0 \quad (13)$$

Where

$$\begin{aligned} a_0 &= c_0 c_{in} k_{i1} T_n L R_s R R_b / (R + R_b) \\ a_1 &= c_0 L (R_0 c_{in} + k_{i1} T_n) R R_b / (R + R_b) + R_s C_{in} K_{i1} T_n L [1 - K_{p1} K_{u1} F_m I_{in} R R_b / (R + R_b)] \\ a_2 &= c_0 (L + R_s K_{i1} T_n) R R_b / (R + R_b) + (1 - D)^2 R_s C_{in} K_{i1} T_n R R_b / (R + R_b) \\ &+ K_{u1} F_m C_{in} K_{i1} T_n R_s (K_{p1} U_{in} - K_{i1} I_{in} L) R R_b / (R + R_b) \\ &+ L [1 - K_{u1} F_m K_{p1} I_{in} R R_b / (R + R_b)] (R_0 C_{in} + K_{i1} T_n) \\ a_3 &= C_0 R_0 R R_b / (R + R_b) + (L + R_s K_{i1} T_n) + (1 - D)^2 (R_0 C_{in} + K_{i1} T_n) R R_b / (R + R_b) \\ &+ K_{u1} F_m K_{p1} [U_{in} (R_0 C_{in} + K_{i1} T_n) - I_{in} (L + R_s K_{i1} T_n)] R R_b / (R + R_b) \\ &+ K_{u1} F_m K_{i1} [U_{in} R_s C_{in} K_{i1} T_n - I_{in} L (R_0 C_{in} + K_{i1} T_n)] R R_b / (R + R_b) \\ a_4 &= R_0 + (1 - D)^2 R R_b / (R + R_b) + K_{u1} F_m K_{p1} (U_{in} - I_{in} R_0) R R_b / (R + R_b) \\ &+ K_{u1} F_m K_{i1} [U_{in} (R_0 C_{in} + K_{i1} T_n) - I_{in} (L + R_s K_{i1} T_n)] R R_b / (R + R_b) \\ a_5 &= K_{u1} F_m K_{i1} (U_{in} - I_{in} R_0) R R_b / (R + R_b) \end{aligned}$$

On the basis of Hurwitz criterion, the necessary stability condition of the system can be described as

$$a_6 = K_{i2} K_{i1} K_{u1} F_m (U_{in} - I_{in} R_0) R R_b / (R + R_b) > 0 \quad (14)$$

Thus, we have

$$F_m (R_{in} - R_0) > 0 \quad (15)$$

Obviously, inequality (15) also is not related to the load type. Based on the same analysis method, we can also come to the following conclusions:

If

$$\begin{cases} \dot{e}_1(s) = k_{u1}\dot{u}_0(s) - \dot{u}_{0,ref}(s) \\ \dot{e}_2(s) = \dot{u}_{in,ref}(s) - k_{u2}\dot{u}_{in}(s) \end{cases}$$

There is

$$F_m (R_{in} - R_0) < 0 \quad (16)$$

If

$$\begin{cases} \dot{e}_1(s) = \dot{u}_{0,ref}(s) - k_{u1}\dot{u}_0(s) \\ \dot{e}_2(s) = k_{u2}\dot{u}_{in}(s) - \dot{u}_{in,ref}(s) \end{cases}$$

There is

$$F_m (R_{in} - R_0) < 0 \quad (17)$$

If

$$\begin{cases} \dot{e}_1(s) = \dot{u}_{0,ref}(s) - k_{u1}\dot{u}_0(s) \\ \dot{e}_2(s) = k_{u2}\dot{u}_{in}(s) - \dot{u}_{in,ref}(s) \end{cases} \quad (18)$$

There is

$$F_m (R_{in} - R_0) > 0 \quad (19)$$

**d) Relations between the control loop formation of interface converter in OVR mode and the stable operating area of PV cells**

As seen from (4), Gud2(s) is negative, which demonstrates that a decrease in the duty ratio D increases the input voltage Uin. Consequently,

If  $\dot{e}_2(s) = \dot{u}_{in,ref}(s) - K_{u2}\dot{u}_{in}(s)$ , the PWM modulator gain Fm must be negative, otherwise the input voltage closed-loop control will be instable. Similarly,

If  $\dot{e}_2(s) = K_{u2}\dot{u}_{in}(s) - \dot{u}_{in,ref}(s)$ , we will have Fm > 0

Besides, literature implies that PV cells will operate at MPP when its output resistance Ro equals the load input resistance Rin, operate in VA when Ro < Rin and operate in CA when Ro > Rin. Therefore, according to the necessary stability conditions described in Sections 4.2 and 4.3, we can get the relations between the control loop formation of interface converter in OVR mode and the stable operating area of PV cells, as shown in Table 2. From Table 2, we can see that the stable operating area of PV cells changes with the variation of the control loop formation of the interface converter in OVR mode. In other words, the control loop formation of the interface converter is the key factor influencing the stable operating



area of PV cells in OVR mode, which answers question (ii) proposed in Section 1.

Furthermore, we can also find that whatever the control loop formation is adopted, the case of  $R_{in} = R_o$  does not appear. This is because  $a_5$  and  $a_6$  shown in (7) and (13) will be equal to zero once  $R_{in} = R_o$ . According to Hurwitz stability criterion, in this case the interface converter in OVR mode must be unstable. That is, the interface converter in OVR mode cannot operate stably when the PV cells are at MPP ( $R_{in} = R_o$ ). In turn, the interface converter in OVR mode cannot make the stable operation point of PV cells reach MPP finally, although in theory it can be infinitely close to MPP. Therefore, PV cells can never output the true maximum power when the interface converter works in OVR mode, which means the answer of question (i) proposed in Section 1 is 'NO'!

made without electrical connections to the rotor as are found in universal, DC and synchronous motors. An asynchronous motor's rotor can be either wound type or squirrel-cage type.

Three-phase squirrel-cage asynchronous motors are widely used in industrial drives because they are rugged, reliable and economical. Single-phase induction motors are used extensively for smaller loads, such as household appliances like fans. Although traditionally used in fixed-speed service, induction motors are increasingly being used with variable-frequency drives (VFDs) in variable-speed service. VFDs offer especially important energy savings opportunities for existing and prospective induction motors in variable-torque centrifugal fan, pump and compressor load applications. Squirrel cage induction motors are very widely used in both fixed-speed and variable-frequency drive (VFD) applications. Variable voltage and variable frequency drives are also used in variable-speed service.

In both induction and synchronous motors, the AC power supplied to the motor's stator creates a magnetic field that rotates in time with the AC oscillations.

**Table 2: Relations between the control loop formation of interface converter in OVR mode and the stable operating area of PV cells**

Control loop formation	Feedback control methods	Necessary stability condition	Modulator gain	Resistance matching	Operating area of PV cells
output voltage single-closed-loop control	$\tilde{u}_d(s) = \tilde{u}_{ref}(s) - K_{v1}\tilde{u}_d(s)$	$F_o/R_o - R_i > 1$	$F_m < 1$	$R_o < R_i$	OA
	$\tilde{u}_q(s) = \tilde{u}_{ref}(s) - K_{v2}\tilde{u}_q(s)$	$F_o/R_o - R_i > 1$	$F_m > 1$	$R_o > R_i$	VA
	$\tilde{u}_d(s) = \tilde{u}_{ref}(s) - K_{v1}\tilde{u}_d(s)$	$F_o/R_o - R_i > 1$	$F_m > 1$	$R_o > R_i$	VA
	$\tilde{u}_q(s) = \tilde{u}_{ref}(s) - K_{v2}\tilde{u}_q(s)$	$F_o/R_o - R_i < 1$	$F_m < 1$	$R_o < R_i$	OA
	$\tilde{u}_d(s) = \tilde{u}_{ref}(s) - K_{v1}\tilde{u}_d(s)$	$F_o/R_o - R_i < 1$	$F_m > 1$	$R_o > R_i$	VA
	$\tilde{u}_q(s) = \tilde{u}_{ref}(s) - K_{v2}\tilde{u}_q(s)$	$F_o/R_o - R_i < 1$	$F_m < 1$	$R_o < R_i$	OA
output-input voltage double-closed-loop control	$\tilde{u}_d(s) = \tilde{u}_{ref}(s) - K_{v1}\tilde{u}_d(s)$	$F_o/R_o - R_i > 1$	$F_m < 1$	$R_o < R_i$	OA
	$\tilde{u}_q(s) = \tilde{u}_{ref}(s) - K_{v2}\tilde{u}_q(s)$	$F_o/R_o - R_i < 1$	$F_m > 1$	$R_o > R_i$	OA
	$\tilde{u}_d(s) = \tilde{u}_{ref}(s) - K_{v1}\tilde{u}_d(s)$	$F_o/R_o - R_i < 1$	$F_m < 1$	$R_o < R_i$	OA
	$\tilde{u}_q(s) = \tilde{u}_{ref}(s) - K_{v2}\tilde{u}_q(s)$	$F_o/R_o - R_i > 1$	$F_m > 1$	$R_o > R_i$	VA
	$\tilde{u}_d(s) = \tilde{u}_{ref}(s) - K_{v1}\tilde{u}_d(s)$	$F_o/R_o - R_i > 1$	$F_m > 1$	$R_o > R_i$	VA
	$\tilde{u}_q(s) = \tilde{u}_{ref}(s) - K_{v2}\tilde{u}_q(s)$	$F_o/R_o - R_i > 1$	$F_m < 1$	$R_o < R_i$	OA

**V. INDUCTION MOTOR**

An asynchronous motor type of an induction motor is an AC electric motor in which the electric current in the rotor needed to produce torque is obtained by electromagnetic induction from the magnetic field of the stator winding. An induction motor can therefore be

Whereas a synchronous motor's rotor turns at the same rate as the stator field, an induction motor's rotor rotates at a slower speed than the stator field. The induction motor stator's magnetic field is therefore changing or rotating relative to the rotor. This induces an opposing current in the induction motor's rotor, in effect the motor's secondary winding, when the latter is short-circuited or closed through external impedance. The rotating magnetic flux induces currents in the windings of the rotor; in a manner similar to currents induced in a transformer's secondary winding(s).

The currents in the rotor windings in turn create magnetic fields in the rotor that react against the stator field. Due to Lenz's Law, the direction of the magnetic field created will be such as to oppose the change in current through the rotor windings. The cause of induced current in the rotor windings is the rotating stator magnetic field, so to oppose the change in rotor-winding currents the rotor will start to rotate in the direction of the rotating stator magnetic field. The rotor accelerates until the magnitude of induced rotor current and torque balances the applied load. Since rotation at synchronous speed would result in no induced rotor current, an induction motor always operates slower than synchronous speed. The difference, or "slip," between actual and



synchronous speed varies from about 0.5 to 5.0% for standard Design B torque curve induction motors. The induction machine's essential character is that it is created solely by induction instead of being separately excited as in synchronous or DC machines or being self-magnetized as in permanent magnet motors.

For rotor currents to be induced the speed of the physical rotor must be lower than that of the stator's rotating magnetic field ( $n_s$ ); otherwise the magnetic field would not be moving relative to the rotor conductors and no currents would be induced. As the speed of the rotor drops below synchronous speed, the rotation rate of the magnetic field in the rotor increases, inducing more current in the windings and creating more torque. The ratio between the rotation rate of the magnetic field induced in the rotor and the rotation rate of the stator's rotating field is called slip. Under load, the speed drops and the slip increases enough to create sufficient torque to turn the load. For this reason, induction motors are sometimes referred to as asynchronous motors. An induction motor can be used as an induction generator, or it can be unrolled to form a linear induction motor which can directly generate linear motion.

**Synchronous Speed:**

The rotational speed of the rotating magnetic field is called as synchronous speed.

$$N_s = \frac{120 \times f}{P} \text{ (RPM)} \tag{20}$$

Where, f = frequency of the supply  
P = number of poles

**Slip:**

Rotor tries to catch up the synchronous speed of the stator field, and hence it rotates. But in practice, rotor never succeeds in catching up. If rotor catches up the stator speed, there won't be any relative speed between the stator flux and the rotor, hence no induced rotor current and no torque production to maintain the rotation. However, this won't stop the motor, the rotor will slow down due to lost of torque, and the torque will again be exerted due to relative speed. That is why the rotor rotates at speed which is always less the synchronous speed. The difference between the synchronous speed ( $N_s$ ) and actual speed ( $N$ ) of the rotor is called as slip.

$$\% \text{ slip } s = \frac{N_s - N}{N_s} \times 100 \tag{21}$$

**VI. MATLAB/SIMULINK RESULTS**

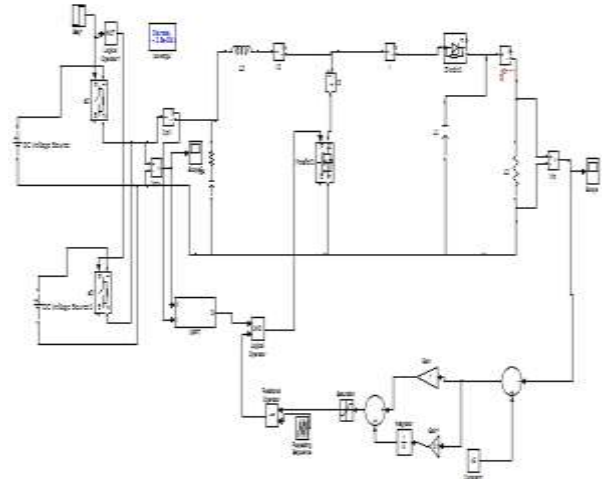


Fig.5 MATLAB/SIMULINK circuit for PV power generation system's structure

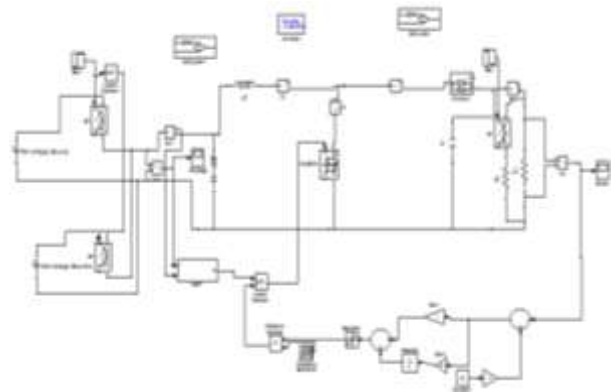


Fig6: MATLAB/SIMULINK circuit for controllers are arranged to work In separately

Fig7: Experiment waveforms when controllers are arranged to work in separately (10 V/div, 250 ms/div)

$$(a) \dot{e}_1(s) = \dot{u}_{0,ref}(s) - k_{u1} \dot{u}_0(s) \text{ and } \dot{e}_2(s) = \dot{u}_{in,ref}(s) - k_{u2} \dot{u}_{in}(s)$$



(i) Constant current load



(ii) Constant resistor load



(iii) Quasi-constant voltage load

$$(b) \dot{e}_1(s) = \dot{u}_{0,ref}(s) - k_{u1} \dot{u}_0(s) \text{ and } \dot{e}_2(s) = k_{u2} \dot{u}_{in}(s) - \dot{u}_{in,ref}(s)$$



(i) Constant current load



(ii) Constant resistor load



(iii) Quasi-constant voltage load

$$(c) \dot{e}_1(s) = k_{u1} \dot{u}_0(s) - \dot{u}_{0,ref}(s) \text{ and } \dot{e}_2(s) = \dot{u}_{in,ref}(s) - k_{u2} \dot{u}_{in}(s)$$



(i) Constant current load



(ii) Constant resistor load



(iii) Quasi-constant voltage load

$$(d) \dot{e}_1(s) = k_{u1} \dot{u}_0(s) - \dot{u}_{0,ref}(s) \text{ and } \dot{e}_2(s) = k_{u2} \dot{u}_{in}(s) - \dot{u}_{in,ref}(s)$$



(i) Constant current load



(ii) Constant resistor load



(iii) Quasi-constant voltage load

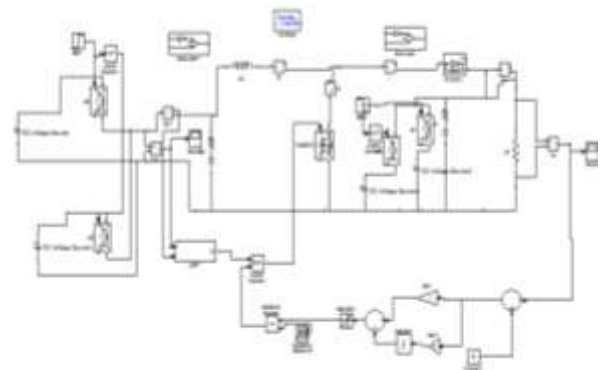


Fig:8 MATLAB/SIMULINK circuit for controllers are arranged to work In series

Fig9: Experiment waveforms when controllers are arranged to work in series



$$(a) \dot{e}_1(s) = \dot{u}_{0,ref}(s) - k_{u1} \dot{u}_0(s) \text{ and } \dot{e}_2(s) = \dot{u}_{in,ref}(s) - k_{u2} \dot{u}_{in}(s) (10 \text{ V/div}, 250 \text{ ms/div})$$



(i) Constant current load



(ii) Constant resistor load



(iii) Quasi-constant voltage load

$$(b) \dot{e}_1(s) = \dot{u}_{0,ref}(s) - k_{u1} \dot{u}_0(s) \text{ and } \dot{e}_2(s) = k_{u2} \dot{u}_{in}(s) - \dot{u}_{in,ref}(s) (10 \text{ V/div}, 2.5 \text{ s/div})$$



(i) Constant current load



(ii) Constant resistor load



(iii) Quasi-constant voltage load

$$(c) \dot{e}_1(s) = k_{u1} \dot{u}_0(s) - \dot{u}_{0,ref}(s) \text{ and } \dot{e}_2(s) = \dot{u}_{in,ref}(s) - k_{u2} \dot{u}_{in}(s) (10 \text{ V/div}, 250 \text{ ms/div})$$



(i) Constant current load



(ii) Constant resistor load



(iii) Quasi-constant voltage load

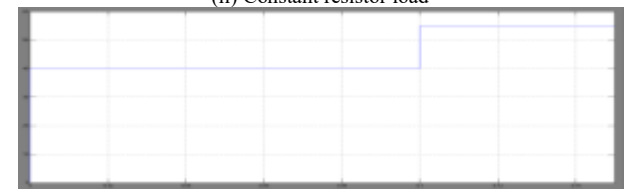
$$(d) \dot{e}_1(s) = k_{u1} \dot{u}_0(s) - \dot{u}_{0,ref}(s) \text{ and } \dot{e}_2(s) = k_{u2} \dot{u}_{in}(s) - \dot{u}_{in,ref}(s) (10 \text{ V/div}, 250 \text{ ms/div})$$



(i) Constant current load



(ii) Constant resistor load



(iii) Quasi-constant voltage load

Fig.10 Experiment waveforms when output voltage single closed-loop control is only adopted (10 V/div, 250 ms/div)

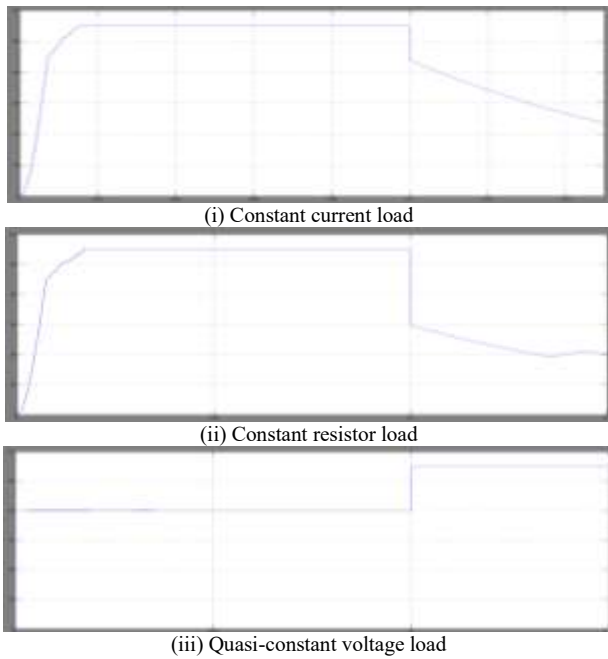


Fig.11 Simulation waveforms when input voltage closed-loop control is only adopted

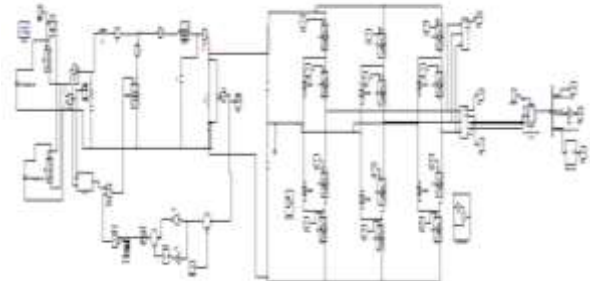
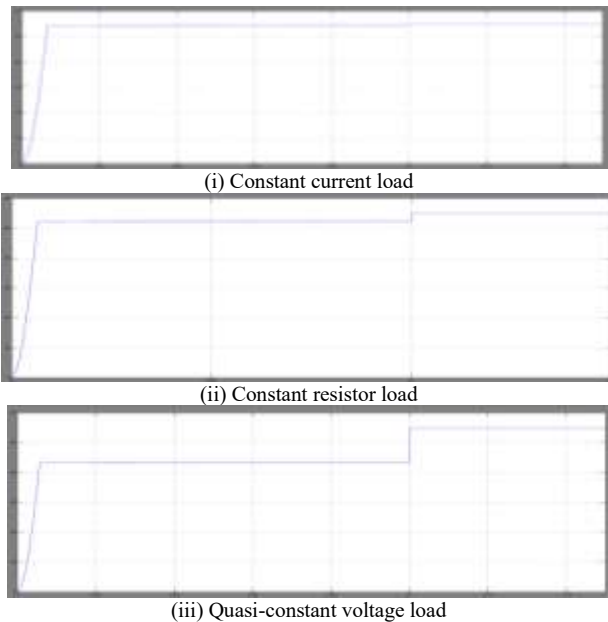


Fig.12 shows the mat lab/Simulink model of proposed system with induction motor drive

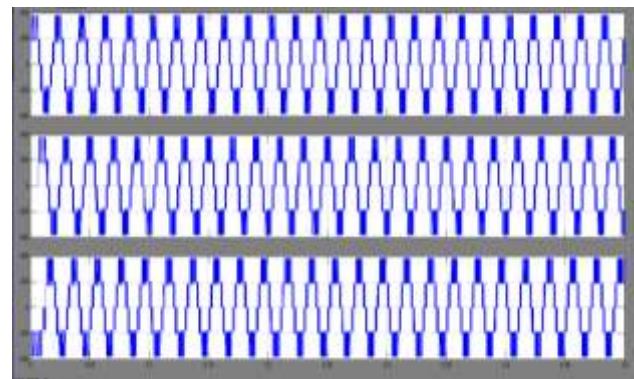


Fig.13 shows the five level inverter line voltage

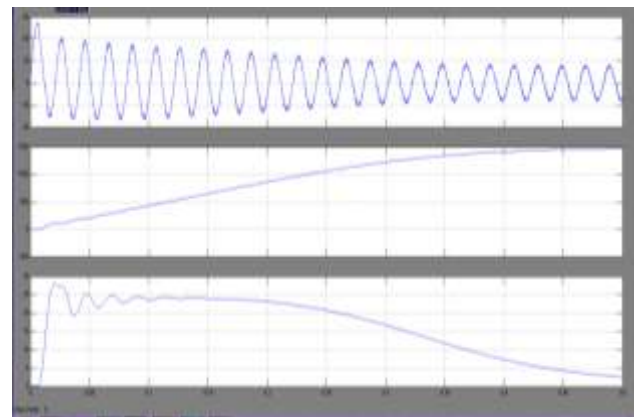


Fig.14 shows the induction motor performance like stator current, speed and torque

**VII. CONCLUSION**

In this paper we present an effective method to drive a three-phase squirrel cage induction motor fed from a single solar PV panel. Based on simulation result we demonstrate that the induction motor can be effectively



driven by a PV panel. Maximum power is extracted effectively from panel using MPPT (P&O) technique with DC-DC converter. The advantage of this DC-DC converter is simple, low cost and high efficiency. This paper has presented the simulation analysis of steady value related consideration, for the proposed converter operated under closed loop manner. The analysis of DC-DC converter integrated inverter feeding induction motor drive is carried out and simulation results are presented. The motor speed is controlled by controlling the switching sequence of the Multilevel Inverter and also by increasing the level of Multilevel Inverter the efficiency of the system is increased.

[10] Suntio, T., Leppäaho, J., Huusari, J.: 'Issues on solar-generator interfacing with voltage-fed converters'. IEEE Power Electronics and Motion Control Conf., Ohrid, Macedonia, 2010, pp. 595–600.

[11] Razzak, M.A. ; Chowdhury, A.S.K. ; Salam, K.M.A., "Induction motor drive system using Push-Pull converter and three-phase SPWM inverter fed from solar photovoltaic panel," Power and Energy Systems Conference: Towards Sustainable Energy, 2014, pp: 1-6.

[12] Mahrous Ahmed, Mostafa Mousa, Mohamed Orabi, "Development of High Gain and Efficiency Photovoltaic System Using Multilevel Boost Converter Topology", The 2nd International Symposium on Power Electronics for Distributed Generation Systems, 16-18 June 2010, Hefei, Anhui, China.

## REFERENCES:

- [1] S. M. Chen, T. J. Liang, L. S. Yang, and J. F. Chen, "A cascaded high stepup dc-dc converter with single switch for micro source applications," IEEE Trans. Power Electron., vol. 26, no. 4, pp. 1146–1153, Apr. 2011.
- [2] W. Li, X. Li, Y. Deng, J. Liu, and X. He, "A review of non-isolated high step-up dc/dc converters in renewable energy applications", 24th Annual Applied Power Electronics Conf. and Exposition (APEC) IEEE 1, pp: 364–369 year: 2009.
- [3] Neha Adhikari, Bhim Singh, A. L. Vyas, Ambrish Chandra Kamal-AIHaddad, "Analysis and Design of Isolated Solar-PV Energy Generating System", IEEE, year: 2011.
- [4] Mahajan Sagar Bhaskar Ranjana, Nandyala Sree ramula Reddy and Repalle KusalaPavan Kumar "Non-Isolated Dual Output Hybrid DC-DC Multilevel Converter for Photovoltaic Applications", 2nd International Conference on Devices, Circuits and Systems (ICDCS), 2014.
- [5] J. T. Bialasiewicz, "Renewable energy systems with photovoltaic power generators: Operation and modeling," IEEE Trans. Ind. Electron., vol. 55, no. 7, pp. 2752–2758, year: Jul. 2008.
- [6] Villalva, M.G., de Siqueira, T.G., Ruppert, E.: 'Voltage regulation of photovoltaic arrays: small-signal analysis and control design', IET Power Electron., 2010, 3, (6), pp. 869–880
- [7] Qin, L., Xie, S., Yang, C., et al.: 'The interfacing stability of photovoltaic cells and current-fed MPPT converter'. IEEE ECCE Asia Downunder, Melbourne, Australia, 2013, pp. 877–881
- [8] Bae, H., Lee, J., Park, S., et al.: 'Large-signal stability analysis of solar array power system', IEEE Trans. Aerosp. Electron. Syst., 2008, 44, (2), pp. 538–547
- [9] Yang, J.H., Bae, H.S., Lee, J.H., et al.: 'A simplified series-parallel structure for the regulated peak power tracking (RPPT) system'. IEEE Applied Power Electronics Conf. and Exposition, Austin, USA, 2008, pp. 877–881